Proceedings of the 33rd Chinese Control Conference
July 28-30, 2014, Nanjing, China

Active Robust Control Scheme for Uncertainty and Flexibility Suppression of Air-breathing Hypersonic Vehicles

PU Zhiqiang[1], YUAN Ruyi[1], TAN Xiangmin[1], and YI Jianqiang[1]

1. Institute of Automation, Chinese Academy of Sciences, Beijing 100190, China
E-mail: zhiqiang.pu@ia.ac.cn

Abstract: Inevitable uncertainties and cross couplings between rigid and flexible modes pose huge challenges to control design for flexible air-breathing hypersonic vehicles. This paper addresses an active robust control scheme that can simultaneously suppress uncertainties and flexible modes using active approaches rather than inherent system robustness. Couplings between different rigid and flexible modes are analyzed, providing insights into internal coupling behaviors. Generally, the active robust control scheme consists of two components: a nonlinear extended state observer (ESO) and a notch filter. The ESO is designed to estimate and compensate diverse uncertainties. For specific high-frequency uncertainties, the ESO estimated values could excite the flexible modes and then cause instabilities. So the notch filter is designed to actively suppress the specific high-frequency estimated signals induced by ESO. Both nonlinear and linear approaches are discussed for the notch filter design. At last, several representative simulations are conducted to demonstrate the advantages of the proposed active robust control scheme.

Key Words: Active control, Uncertainty, Flexibility suppression, Hypersonic vehicle, Extended state observer, Notch filter

1 Introduction

Air-breathing hypersonic vehicles have been drawing lots of attentions in recent decades because of their dramatic advantages such as fast flight speed, large payload, good cost-effectiveness, etc. However, it is still a long way for practical and affordable full scale vehicles to be used in real applications due to their peculiar dynamic behaviors. These vehicles usually consist of long, slender configurations with light materials, causing noticeable flexible modes that own much slower frequencies than normal aircraft [1, 2, 3]. Significant couplings therefore exist between rigid and flexible modes, which may cause instabilities and even potential structural damages. Besides the flexibility effects, uncertainties and disturbances exist inevitably in practical applications because of complex, even unknown vehicle behaviors and environment features during large flight envelopes [4, 5, 6]. In fact, the uncertainty effects are tightly connected with the flexibility effects. For example, some high-frequency uncertainties could excite the flexible modes and, in return, the excited flexibility effects could generate larger uncertainties. Interactions of the rigid-body dynamics, flexible modes, controls, and extra uncertainties can be illustrated as Fig. 1.

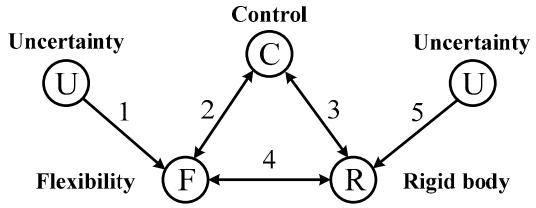

Fig. 1: Interactions of the rigid-body dynamics, flexible modes, controls, and extra uncertainties

A robust control scheme should be adequately designed that can simultaneously suppress the aforementioned flexible modes and diverse uncertainties for a flexible air-breathing hypersonic vehicle (FAHV). In the literature, several results on the analysis of mutual interactions among inertial, elastic, and aerodynamic forces were obtained [1, 2]. However, control design that actively dealt with flexible modes received far less attentions. Robust control systems were designed in [5, 6] for a generic hypersonic vehicle which was modeled as a pure rigid body, while flexibility was not included. As for FAHVs, linear quadratic regulator [7] and nonlinear adaptive inversion [8] were adopted for the first-principle vehicle model developed by Bolender and Doman [3]. In these literatures, the flexibility effects were implicitly rejected by inherent system robustness. This idea is applicable only when the flexible modes are not excited thus the coupling effects are not severe enough. For another vehicle model of Mirmirani et al. [9], [10] designed a notch filter that acted on the control inputs so as to actively suppress the flexible modes, while uncertainty rejection was not considered. As for the uncertainty rejection problem, many literatures that took this issue into consideration were only for the purpose of verifying the system robustness, thus no active approaches were taken for direct rejection.

Building upon our recent work on uncertainty modeling and analysis [11], we present here an active robust control scheme for uncertainty and flexible modes suppression of the FAHV model by Bolender and Doman [3]. In this scheme, uncertainty compensation control law based on nonlinear observers is firstly designed to actively suppress the uncertainty effects in Path 1 and 5, illustrated as Fig. 1. However, if the uncertainties contain specific high-frequency components, the compensation law may achieve an opposite result: they may excite the flexible modes. To suppress the potential excitation effect of the estimated signals, notch filters are further designed subsequent to the uncertainty observers. Illustrated by Fig. 1, this flexibility suppression effect is achieved by attenuating (if not completely canceling) the flexibility couplings on Path 2 and Path 3. In result, the active robust scheme makes a tradeoff between uncertainty compensation performance and flexibility suppression. Therefore, both uncertainties and flexible modes can be actively suppressed (not implicitly suppressed by inherent system robustness).

*This work is supported by National Natural Science Foundation (NNSF) of China (Grants No. 61273149, 61203003, 61273336) and the Special Project for Innovation Methods of MOST (Grant No. 2012IM010200).

As for control method in the active control scheme, nonlinear dynamic inversion (NDI) [5, 12] is adopted to design a stabilizing control frame. Its inherent drawback of requiring exact model dynamics is counteracted by uncertainty observation and compensation. The uncertainty observer is implemented by the extended state observer (ESO) technique [13, 14]. ESO utilizes nonlinear structures, exhibiting high efficiency of estimating both internal and external disturbances. Its great simplicity can significantly shorten on-line computing time and meet fast computation requirement in practical hypersonic missions. ESO can also perform as a good low-pass filter, thus can be used to design the notch filter. In this paper, both ESO and a linear approach are utilized to design notch filters, and their differences are also investigated.

2 Model Description

The vehicle studied in this paper is the longitudinal FAHV model developed by Bolender and Doman [3]. Flexibility effects are included by modeling the fuselage as a free-free beam so that the flexible modes are orthogonal to the rigid-body modes and the coupling effects between the flexible and rigid dynamics occur through the forces and moments [15]. Assuming a flat Earth and normalizing the vehicle to unit depth, the nominal motion equations of FAHV without extra disturbances are described as

$$\dot{V} = (T\cos\alpha - D)/m - g\sin\gamma \tag{1}$$

$$\dot{\gamma} = (L + T\sin\alpha)/(mV) - g\cos\gamma/V \tag{2}$$

$$\dot{h} = V\sin\gamma \quad (3) \qquad \dot{\alpha} = Q - \dot{\gamma} \quad (4) \qquad \dot{Q} = M/I_{yy} \quad (5)$$

$$\ddot{\eta}_i = -2\xi_i\omega_i\dot{\eta}_i - \omega_i^2\eta_i + N_i, \quad i = 1,2,3 \tag{6}$$

This model consists of five rigid-body flight states $\boldsymbol{x} = [V, \gamma, h, \alpha, Q]^T$, where V, γ, h, α, Q are the velocity, flight-path angle (FPA), altitude, angle of attack (AOA), and pitch rate, respectively. It also includes six flexible states $\boldsymbol{\eta} = [\eta_1, \dot{\eta}_1, \eta_2, \dot{\eta}_2, \eta_3, \dot{\eta}_3]^T$ corresponding to the first three flexible modes and their derivatives. Modal frequencies are set as $\omega_1 = 21.17$ rad/sec, $\omega_2 = 53.92$ rad/sec, and $\omega_3 = 109.1$ rad/sec [7]. The damping ratio is constant: $\xi_i = 0.02$, indicating a severe mode vibration. The canard deflection δ_c is ganged with the elevator deflection δ_e with a negative gain k_{ec}: $\delta_c = k_{ec}\delta_e$ [8]. Therefore, the control input that needs control law design is $\boldsymbol{u} = [\delta_e, \phi]^T$, where ϕ is the fuel equivalence ratio. The output to be controlled is selected as $\boldsymbol{y} = [V, h]^T$. The lift L, drag D, thrust T, pitching moment M, and generalized forces N_i are complicated nonlinear functions of the flight states and control inputs. For the sake of control design and stability analysis, Fiorentini [15] developed a control design model (CDM) to approximate the forces and moment based on curve fitting, where ($i = 1,2,3$)

$$\begin{cases} T \approx \bar{q}S[C_{T,\phi}(\alpha)\phi + C_T(\alpha) + \boldsymbol{C}_T^{\eta}\boldsymbol{\eta}] \\ L \approx \bar{q}SC_L(\alpha,\boldsymbol{\delta},\boldsymbol{\eta}), \quad D \approx \bar{q}SC_D(\alpha,\boldsymbol{\delta},\boldsymbol{\eta}) \\ M \approx z_T T + \bar{q}S\bar{c}C_M(\alpha,\boldsymbol{\delta},\boldsymbol{\eta}) \\ N_i \approx \bar{q}S[N_i^{\alpha^2}\alpha^2 + N_i^{\alpha}\alpha + N_i^{\delta_e}\delta_e + N_i^{\delta_c}\delta_c + N_i^0 + \boldsymbol{N}_i^{\eta}\boldsymbol{\eta}] \end{cases} \tag{7}$$

where $\boldsymbol{\delta} = [\delta_c, \delta_e]^T$, and the coefficients are expressed as

$$\begin{cases} C_{T,\phi}(\alpha) = C_T^{\phi\alpha^3}\alpha^3 + C_T^{\phi\alpha^2}\alpha^2 + C_T^{\phi\alpha}\alpha + C_T^{\phi} \\ C_T(\alpha) = C_T^3\alpha^3 + C_T^2\alpha^2 + C_T^1\alpha + C_T^0 \\ C_L(\alpha,\boldsymbol{\delta},\boldsymbol{\eta}) = C_L^{\alpha}\alpha + C_L^{\delta_e}\delta_e + C_L^{\delta_c}\delta_c + C_L^0 + \boldsymbol{C}_L^{\eta}\boldsymbol{\eta} \\ C_D(\alpha,\boldsymbol{\delta},\boldsymbol{\eta}) = C_D^{\alpha^2}\alpha^2 + C_D^{\alpha}\alpha + C_D^{\delta_e^2}\delta_e^2 + C_D^{\delta_e}\delta_e \\ \qquad + C_D^{\delta_c^2}\delta_c^2 + C_D^{\delta_c}\delta_c + C_D^0 + \boldsymbol{C}_D^{\eta}\boldsymbol{\eta} \\ C_M(\alpha,\boldsymbol{\delta},\boldsymbol{\eta}) = C_M^{\alpha^2}\alpha^2 + C_M^{\alpha}\alpha + C_M^{\delta_e}\delta_e + C_M^{\delta_c}\delta_c \\ \qquad + C_M^0 + \boldsymbol{C}_M^{\eta}\boldsymbol{\eta} \\ \boldsymbol{C}_j^{\eta} = \begin{bmatrix} C_j^{\eta_1} & 0 & C_j^{\eta_2} & 0 & C_j^{\eta_3} & 0 \end{bmatrix}, \ j = T, L, D, M \\ \boldsymbol{N}_i^{\eta} = \begin{bmatrix} N_i^{\eta_1} & 0 & N_i^{\eta_2} & 0 & N_i^{\eta_3} & 0 \end{bmatrix}, \ i = 1,2,3 \end{cases} \tag{8}$$

The reader is referred to [15] for a full description of the model variables and their numerical values. The dynamic pressure is calculated as $\bar{q} = 0.5\rho V^2$, where the air density ρ is modeled as $\rho = \rho_0 \exp(-h/h_0)$ with $\rho_0 = 1.2266$ kg/m^3 and $h_0 = 7315.2$ m. Actuators are modeled as first-order low-pass filters with certain gains. Limits on the actuator outputs are set as

$$-20 \text{ deg} \le \delta_c, \delta_e \le 20 \text{ deg}, \quad 0.05 \le \phi \le 1.5 \tag{9}$$

Diverse uncertainties exist inevitably in practical flight. In our recent work [11], major uncertainties were divided into four categories: uncertainties relevant to flexibility, environment, rigid-body aerodynamic coefficients, and control-oriented modeling errors. Then a uniform uncertain model based on the nominal model (1)-(6) can be derived as

$$\left[\dot{\boldsymbol{x}}, \dot{\boldsymbol{\eta}}\right]^T = \boldsymbol{f}(\boldsymbol{x},\boldsymbol{\eta},\boldsymbol{u},t) + \sum_{i=1}^{4}\boldsymbol{f}_{\Delta i}(\boldsymbol{x},\boldsymbol{\eta},\boldsymbol{u},t) \tag{10}$$

where $\boldsymbol{f}(\cdot) \in \Re^{11}$ denotes the nominal dynamics, and $\boldsymbol{f}_{\Delta i}(\cdot)$ represents different uncertainties. Detailed modeling and analysis of the uncertainty can be found in [11].

To assess the cross couplings between rigid and flexible dynamics, frequency response analysis is conducted under the trim condition given in [7]. Set the fuel equivalence ratio fixed. Select the elevator deflection as the single control input and separately set the FPA, altitude, AOA, and pitch rate as the single output. Then linearize the vehicle model at the trim condition. Magnitude frequency responses are given in Fig. 2. It is seen that all of the four rigid modes (especially the FPA and altitude modes) are affected by the flexibility coupling. From an opposite perspective, separately select the three flexible modes as the single output, and still select the elevator deflection as the single control input. Then Fig. 3 shows how the rigid-body dynamics affect the flexible modes. Each plot contains two peaks: one residing at its natural flexibility frequency, the other residing at a common frequency labeled by the ellipses. This common frequency (about 0.0415 rad/sec) is quite close to the frequency of the phugoid modes (0.0404 rad/sec). Therefore, the flexible modes are also significantly affected by the cross coupling from the rigid dynamics. These cross couplings indicated in Figs. 2~3 need to be actively suppressed.

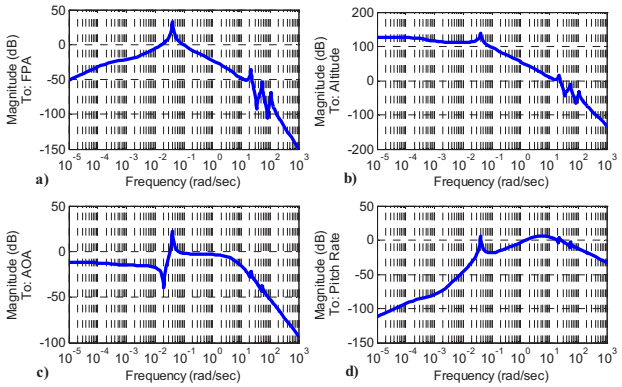

Fig. 2: Magnitude frequency responses from δ_e to rigid modes

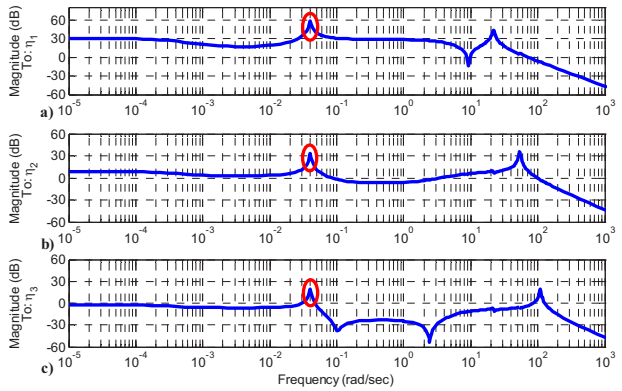

Fig. 3: Magnitude frequency responses from δ_e to flexible modes

3 Active Robust Control Scheme Design

As stated before, the objective of this paper is to simultaneously suppress uncertainties and flexibility couplings in velocity and altitude tracking. The tedious rigid-body motion equations can be decoupled into five functional subsystems, namely, the velocity, altitude, FPA, AOA, and pitch rate subsystems. Accordingly, the overall control scheme consists of five subsystem controllers. Because measurements of the flexible modes are difficult and need additional sensor signals [7], the flexible states are assumed not to be available for feedback. Fig. 4(a) shows the structure of the overall control scheme. Feedback signals are omitted for simplicity. Fig. 4(b) shows the inner structure of each subsystem controller, where $i = V, \gamma, h, \alpha, Q$. NDI and a stabilizer construct a basic stabilizing control law. ESO estimates diverse uncertainties for compensation. The notch filter is integrated to suppress specific high-frequency estimated signals induced by ESO. As shown in Fig. 2, the coupling levels between different rigid-body and flexible modes are quite different, thus the notch filter can be added into a specific subsystem or all of the five subsystems, determined by practical performance. In addition, a command processor based on arranging transient process (ATP) technique is added to reshape the original reference command.

3.1 Stabilizing Control Law Design

In this sub-section, basic stabilizing control laws for the five subsystems are designed based on NDI. A thorough theoretical discussion on NDI can be found in [12].

First consider the velocity subsystem. In view of the drag and thrust expressions in (7)-(8), it can be written as

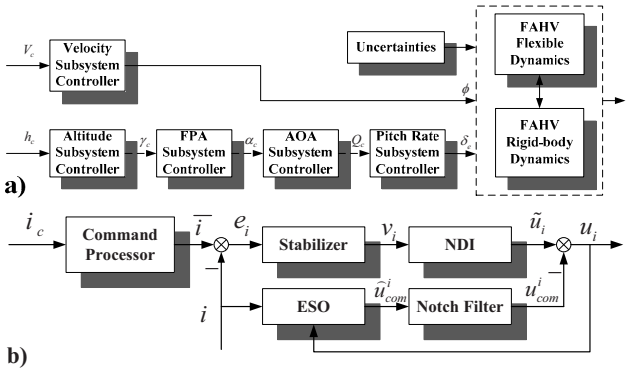

Fig. 4: Block diagram of the active control scheme: a) the overall control scheme; b) Inner structure of each subsystem controller

$$\dot{V} = f_V + g_V \tilde{u}_V + \Delta_{V1} \tag{11}$$

where

$$f_V = \bar{q}S[C_T(\alpha)\cos\alpha - (C_D^{\alpha^2}\alpha^2 + C_D^{\alpha}\alpha + C_D^{\delta_e^2}\delta_e^2 + C_D^{\delta_e}\delta_e + C_D^{\delta_c^2}\delta_c^2 + C_D^{\delta_c}\delta_c + C_D^0)]/m - g\sin\gamma$$

$$g_V = \bar{q}SC_{T,\phi}(\alpha)\cos\alpha / m$$

$$\Delta_{V1} = \bar{q}S(\boldsymbol{C}_T^{\eta}\boldsymbol{\eta}\cos\alpha - \boldsymbol{C}_D^{\eta}\boldsymbol{\eta})/m, \quad \tilde{u}_V = \phi$$

Δ_{V1} denotes the flexibility uncertainty, which is later considered in the observer design. Thus an affine form of the velocity dynamics can be obtained as

$$\dot{V} = f_V + g_V \tilde{u}_V \tag{12}$$

Denote the velocity tracking error as $e_V = V - \bar{V}$, where $\bar{V}$ is the reference velocity command generated by the command processor and has bounded first-order derivative $\dot{\bar{V}}$. The tracking error dynamics can then be derived as

$$\dot{e}_V = f_V + g_V \tilde{u}_V - \dot{\bar{V}} \tag{13}$$

In view of the g_V expression in (11), we can easily verify that g_V is invertible in the whole admissible flight envelope. Thus, select the basic control law as

$$\tilde{u}_V = (v_V - f_V + \dot{\bar{V}})/g_V \tag{14}$$

where v_V is a virtual control input. Substituting (14) into (13) yields a linear velocity tracking error dynamics:

$$\dot{e}_V = v_V \tag{15}$$

The virtual control input v_V can be designed with diverse linear system control methods to stabilize the system (15). A basic state feedback control law as

$$v_V = -k_V e_V \tag{16}$$

gives the closed-loop system as $\dot{e}_V = -k_V e_V$. Thus, choosing $k_V > 0$ can guarantee the closed-loop stability. Substituting (16) back into (14) produces the final basic control law:

$$\tilde{u}_V = (-k_V e_V - f_V + \dot{\bar{V}})/g_V \tag{17}$$

The reference command $\bar{V}$ and its derivative $\dot{\bar{V}}$ are generated by the command processor based on the ATP technique. Compared with the so called “prefilter” which is widely used in current literatures [7, 8], ATP uses only one parameter to feasibly arrange the desired transient process of a reference command and simultaneously generate its first-order derivative. Details about ATP are omitted here to avoid clouding the main idea of this paper, while they can be found in our previous work [11, 16].

Following the procedure (11)-(17), basic control laws for the other four subsystems can be similarly designed, thus their details are omitted.

3.2 Extended State Observer Design

The basic stabilizing control law is designed for the nominal vehicle dynamics. When extra uncertainties are considered, the inherent closed-loop stability margin may shrink and this basic control law may be degraded. Still take the velocity dynamics for demonstration. Based on the uniform uncertain model (10), the disturbed velocity dynamics is assumed to be written as

$$\dot{V} = f_V + g_V u_V + \underbrace{\sum_{i=1}^{4} \Delta_{Vi}}_{\Delta_V} \tag{18}$$

Diverse uncertainties are lumped into a total uncertainty Δ_V. Δ_{V1}, expressed in (11), denotes the flexibility coupling effect, whereas $\Delta_{V2} \sim \Delta_{V4}$ separately denote environmental disturbances, aerodynamic coefficient uncertainties, and control-oriented modeling errors.

Nonlinear ESO is constructed to estimate the total uncertainty in this subsection. The core idea of ESO is to take all internal and external uncertainties as a new extended state, and then establish a nonlinear state observer to estimate these uncertainties. For (18), define $x_{V1} = V$ and $x_{V2} = \Delta_V$. Suppose $\dot{\Delta}_V$=-$w_V(t)$ with $w_V(t)$ unknown but bounded. Then (18) can be written as a second-order extended system:

$$\dot{x}_{V1} = f_V + g_V u_V + x_{V2}, \quad \dot{x}_{V2} = -w_V(t) \tag{19}$$

A nonlinear ESO can be established for (19) as

$$\begin{cases} e_1 = z_{V1} - x_{V1} \\ \dot{z}_{V1} = f_V + g_V u_V + z_{V2} - \beta_{V1} e_1 \\ \dot{z}_{V2} = -\beta_{V2} fal(e_1, \alpha_V, \sigma_V) \end{cases} \tag{20}$$

where z_{Vi} denotes the estimation value of x_{Vi}, e_1 is the velocity estimation error, and $\beta_{Vi} > 0$ is the observer gain, $i = 1, 2$. *fal* is a function of e_1, expressed as [14]

$$fal(e_1, \alpha_V, \sigma_V) = \begin{cases} |e_1|^{\alpha_V} \cdot sign(e_1), & |e_1| > \sigma_V \\ e_1 / \sigma_V^{1-\alpha_V}, & |e_1| \le \sigma_V \end{cases} \tag{21}$$

where σ_V and α_V, subjecting to $\sigma_V > 0$ and $\alpha_V > 0$, are extra parameters needed to be tuned. If $\alpha_V \neq 1$, (21) indicates a nonlinear structure; while if $\alpha_V = 1$, it becomes a normally used linear structure. With proper parameters β_{V1}, β_{V2}, α_V, and σ_V, the estimated values z_{Vi} can be obtained [14]. A thorough investigation on the parameter tuning and stability analysis of the nonlinear ESO can be found in our work [16].

Once the total uncertainty is estimated by z_{V2}, a compensation control law can be designed as

$$u_{com}^V = g_V^{-1} z_{V2} \tag{22}$$

This together with the basic control law (17) yields the total robust control law for the velocity subsystem:

$$u_V = \tilde{u}_V - u_{com}^V \tag{23}$$

ESOs for the other four subsystems can be similarly constructed, thus of which the details are omitted.

Remark 1. By separating the whole rigid-body dynamics into five interconnected subsystems, uncertainties existing in all five channels can be viewed as matched uncertainties and suppressed by ESO. This provides an alternative way to solve the mismatched uncertainty attenuation problem investigated in, for instance, [6].

Remark 2. In the velocity ESO (20), the known model information $f_V + g_V u_V$ can also be lumped as uncertainty. In this sense, ESO is a real model-independent approach for observer design. However, in this paper we separate the known model information from unknown disturbances to decrease the estimating burden of ESO.

3.3 Notch Filter Design

Notch filters are integrated to suppress specific high-frequency compensation signals induced by ESOs to avoid exciting the flexible modes. As reported in [7], the frequencies of flexible modes could be time-varying due to fuel consumption or thermal heating. The uncertain ranges are within about 30% [10]. In this paper, because ESO is adopted to estimate diverse uncertainties (including flexibility uncertainties), the system robustness is notably improved. Therefore, the central frequencies of notch filters are viewed as known and fixed, although in the simulation model the frequencies of the flexible modes are still considered as uncertain. This simplification makes adaptive techniques that aim to estimate the flexible frequencies [10] unnecessary, thus relevant sensors are also unnecessary to avoid introducing additional uncertainties. The central frequencies of the notch filters are chosen as the natural flexible frequencies of the flexible modes.

In fact, ESO can behave not only as an observer, but also as a low-pass filter. Consider a first-order disturbed system

$$\dot{x}_e = \underbrace{f_e(x_e, u_e, t) + \Delta_e}_{\Delta_{e\_tot}} \tag{24}$$

where x_e and u_e are the state and control input, f_e represents the nominal system dynamics, and Δ_e denotes extra disturbance. Lump f_e and Δ_e together as a total disturbance Δ_{e_tot}. For demonstration, suppose $\Delta_{e\_tot} = A_e \sin(\omega_e t)$. Construct an ESO for (24) that is similar to (20), and carefully choose its observation gains β_{e1}, β_{e2} and nonlinear parameters α_e, and σ_e. Then the observed value of Δ_{e_tot} almost converges to another sine signal, denoted as $z_{e2} \approx A_e' \sin[\omega_e (t + \varphi_e)]$. The magnitude and phase of the frequency response of this ESO can be approximated as $(\lg(\omega_e), 20\lg(A_e'/A_e))$ and $(\lg(\omega_e), \varphi)$. Let some parameters fixed as $\beta_{e1} = 15$, $\alpha_e = 0.5$, and $\sigma_e = 5h_0$ where $h_0 = 0.01\,\text{sec}$ is the sampling period. Based on numerical approach, the frequency response of ESO with different β_{e2} and A_e can be depicted as Fig. 5. For $\omega_e < \omega_c$ where ω_c denotes the corner frequency, the amplitude has $A_e'/A_e \approx 1$ and the phase lag is small; for $\omega_e > \omega_c$, the amplitude approaches to a straight line with its slope about -30 dB/dec and the phase lag rapidly decreases to -180°. Thus the ESO behaves as a good low-pass filter. The observer gain has a great impact on the frequency response:

a larger observer gain corresponds to a wider passband. In addition, the amplitude of the input signal also affects the frequency response.

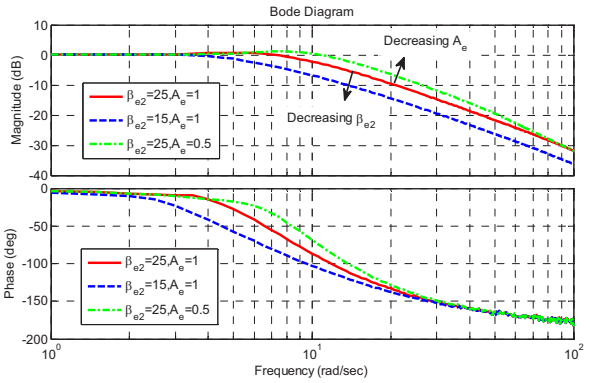

Fig. 5: Bode Diagram of ESO with different β_{e2} and A_e

With proper parameter values, such two ESO based low-pass filters in parallel can construct a notch filter. This approach shows an advantage that the uncertainty observers are simultaneously designed as low-pass filters, thus we do not need to design additional filters subsequent to the ESOs. The drawback lies in that because known model information ($f_V + g_V u_V$ in (20), for example) is explicitly utilized to design the ESO, frequency characteristics of the five ESOs could be different. Thus ESO parameter tuning could be time-consuming. For this consideration, a second approach to notch filter design is presented in this paper, where the notch filter is independently designed to filter the ESO output signals. The notch filter has the linear form as

$$N(s) = \frac{s^2 + \omega_{jk}^2}{s^2 + \omega_{jk} s / Q_{jk} + \omega_{jk}^2} \tag{25}$$

where ω_{jk} and Q_{jk}, $j = V, \gamma, h, \alpha, Q$, $k = 1,2,3$, separately denote the central frequency and quality factor of the notch filter. Here the central frequency is separately chosen as the nominal natural frequencies of the first three flexible modes. A larger quality factor provides a narrower stopband and a smaller phase lag, which is beneficial for expanding the bandwidth of rigid-body controllers. However, due to the uncertainty of the flexible natural frequency and other physical limits, the quality factor cannot be infinitely increased. In this paper, we choose $Q_{jk} = 1$.

A primary advantage of the linear notch filter (25) lies in that the parameters ω_{jk} and Q_{jk} are easy to be tuned, although we need to explicitly design filters apart from the ESOs. In this paper, we finally take this linear approach to the notch filter design, while the nonlinear approach based on ESO is designed as an alternative and also for the theoretical completeness of nonlinear ESO investigation.

4 Simulations

The active robust control scheme has been tested in several representative simulations. The initial trim condition is given in [7]. Parameter values for the five basic NDI controllers, five ESOs, and the notch filters in the altitude and FPA subsystems are given in Table 1, where $j = V, \gamma, h, \alpha, Q$, $k = 1,2,3$. The five ESOs utilize the same set of parameter values, which indicates the great parameter adaption property of nonlinear ESO method.

Table 1: Control parameters

NDI	Value	ESO	Value	Notch filter	Value
k_V	0.1	β_{j1}	15	ω_{j1}	21.17
k_γ	0.9	β_{j2}	15	ω_{j2}	53.92
k_h	0.1	α_j	0.5	ω_{j3}	109.1
k_α	0.6	σ_j	0.02	Q_{jk}	1
k_Q	2.5				

The first simulation studies a constant dynamic pressure case. The altitude command is given to let the vehicle climb from 85000 ft to 95000 ft, while the velocity command is generated by solving the air density model to maintain a constant dynamic pressure (about 2076 psf). Except for the flexibility disturbance, no additional uncertainties are added. Simulation comparisons between the active robust scheme and the scheme that only contains basic NDI control laws are illustrated in Fig. 6. It is seen that for this case, both schemes can stabilize the vehicle. However, due to the weak flexibility disturbance, the basic NDI scheme exhibits a steady velocity tracking error and a worse dynamic process of the altitude tracking error.

Next, the velocity and altitude reference commands are independently given as 10500 ft/sec and 110000 ft, indicating a very large maneuver. Multiple uncertainties are considered. In the first 400 sec, a combination of parameter uncertainty is added, including +40% uncertainty of C_D and -40% uncertainties of $\{C_L, C_{T,\phi}, C_T, C_M\}$. Between 400 sec and 500 sec, environmental disturbances are added to the velocity and pitching rate dynamics. For demonstration, set $\Delta_{V2} = 2\sin t$ and $\Delta_{Q2} = 0.05\sin(2t)$. Besides, the flexibilities are also taken as disturbances to the rigid-body dynamics within the whole simulation. Here we add different categories of uncertainties in different stages to separately test the robustness of the active control scheme to different uncertainties. Comparisons between the robust scheme and the basic NDI scheme are given in Fig. 7. The basic NDI scheme performs a large velocity tracking error and a much worse dynamic process of the altitude tracking error in the parameter uncertainty stage, and also an oscillation in the sine wave disturbance stage. However, the robust scheme performs quite well for all of these uncertainties, mostly due to the excellent uncertainty estimation ability of ESO. The estimation values of the uncertainties in the velocity and pitch rate dynamics are given in Figs. 7(c)-(d).

In the last simulation, a high-frequency disturbance is added to the FPA dynamics between 400 sec to 500 sec, i.e., $\Delta_{\gamma 2} = 0.005\sin(21t)$. The frequency of this disturbance is quite close to the first flexible mode. Simulation results of the control scheme that is without and with the notch filter in the FPA dynamics are depicted in Fig. 8. Without the notch filter, the first flexible mode is excited by the high-frequency estimated signal induced by ESO in the FPA dynamics. Then this excited flexible mode reacts on the rigid dynamics. Following this cross coupling loop, a large oscillation occurs in the altitude tracking; meanwhile, all other flexible modes are also excited. On the contrary, the active robust scheme that contains the notch filter in the FPA dynamics still performs well as the high-frequency signal is suppressed by the notch filter. Therefore, the altitude tracking is not influenced; meanwhile, the

oscillation of the first mode is kept small and the other two flexible modes are not excited.

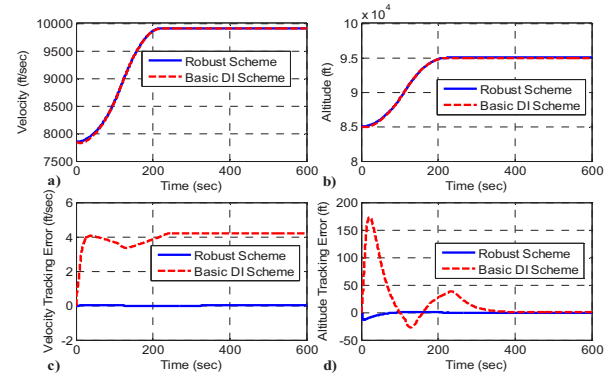

Fig. 6: Simulation with no additional uncertainties

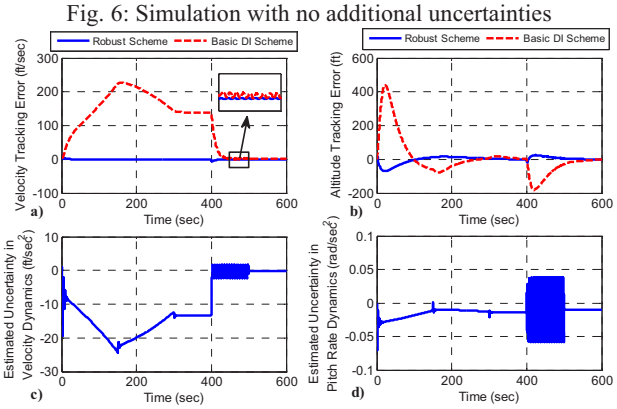

Fig. 7: Simulation with multiple uncertainties

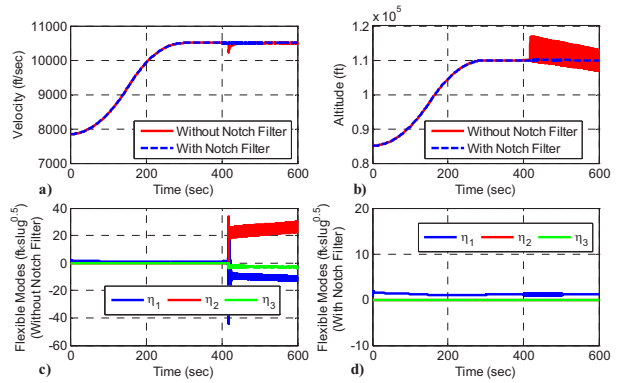

Fig. 8: Simulation with high-frequency disturbance added to the FPA dynamics

5 Conclusions

Robustness enhancement to significant uncertainties and strong flexibility couplings is a challenging task for the control system design of FAHVs. Differing from most of current researches, where the uncertainties and flexibilities are implicitly suppressed by the inherent system robustness, this paper presents an active robust control scheme that can simultaneously suppress diverse uncertainties and the flexible cross couplings. In this scheme, the nonlinear ESOs estimate the uncertainties to form compensation laws, and the notch filters suppress the high-frequency estimated signals that could excite the flexible modes and strengthen the cross couplings. It is noteworthy that as the coupling levels between different rigid-body and flexible modes are quite different, the notch filters can be added into some specific subsystem controllers or all of the five subsystems, determined by practical performances. This strategy makes a good tradeoff between uncertainty compensation and flexibility suppression. Simulations have demonstrated the effectiveness of the active robust control scheme.

References

[1] T. Williams, M. A. Bolender, D. B. Doman, and O. Morataya, An aerothermal flexible mode analysis of a hypersonic vehicle, in *AIAA Atmospheric Flight Mechanics Conference and Exhibit*, 2006, AIAA 2006-6647.

[2] J. J. McNamara and P. P. Friedmann, Aeroelastic and aerothermoelastic analysis of hypersonic vehicles: current status and future trends, in *AIAA/ASME/ASCE/AHS/ASC Structures, Structural Dynamics, and Materials Conference*, 2007, AIAA 2007-2013.

[3] M. A. Bolender and D. B. Doman, Nonlinear longitudinal dynamical model of an air-breathing hypersonic vehicle, *Journal of Spacecraft and Rockets*, 44(2): 374-387, 2007.

[4] F. R. Chavez and D. K. Schmidt, Uncertainty modeling for multivariable-control robustness analysis of elastic high-speed vehicles," *Journal of Guidance, Control, and Dynamics*, 22(1): 87-95, 1999.

[5] H. Xu, M. D. Mirmirani, and P. A. Ioannou, Adaptive sliding mode control design for a hypersonic flight vehicle," *Journal of Guidance, Control, and Dynamics*, 27(5): 829-838, 2004.

[6] J. Yang, S. Li, C. Sun, and L. Guo, Nonlinear-disturbance-observer-based robust flight control for airbreathing hypersonic vehicles, *IEEE Transactions on Aerospace and Electronic Systems*, 49(2): 1263-1275, 2013.

[7] D. O. Sigthorsson, P. Jankovsky, A. Serrani, S. Yurkovich, M. A. Bolender, and D. B. Doman, Robust linear output feedback control of an airbreathing hypersonic vehicle, *Journal of Guidance, Control, and Dynamics*, 29(2): 1052-1066, 2008.

[8] L. Fiorentini, A. Serrani, M. A. Bolender, and D. B. Doman, Nonlinear robust adaptive control of flexible air-breathing hypersonic vehicles, *Journal of Guidance, Control, and Dynamics*, 32(2): 401-416, 2009.

[9] M. Mirmirani, C. Wu, A. Clark, S. Choi, and R. Colgren, Modeling for control of a generic airbreathing hypersonic vehicle, in *AIAA Guidance, Navigation, and Control Conference and Exhibit*, 2005, AIAA 2005-6256.

[10] J. Levin, P. Ioannou, and M. Mirmirani, Adaptive mode suppression scheme for an aeroelastic airbreathing hypersonic cruise vehicle, in *AIAA Guidance, Navigation, and Control Conference and Exhibit*, 2008, AIAA 2008-7137.

[11] Z. Pu, X. Tan, G. Fan, and J. Yi, Uncertainty analysis and robust trajectory linearization control of a flexible air-breathing hypersonic vehicle, *Acta Astranautica*, accepted.

[12] K. K. Hassan, *Nonlinear Systems*, 3rd ed., Prentice Hall Press, Upper Saddle River, New Jersey, 2001, chapter 13.

[13] Z. Gao, Y. Huang, and J. H, An alternative paradigm for control system design, in *Proceedings of the 40th IEEE Conference on Decision and Control*, 2001: 4578-4585.

[14] J. Han, *Active Disturbance Rejection Control Technique-The Technique for Estimating and Compensating the Uncertainties*, National Defense Industry Press, Beijing, 2009. (In Chinese)

[15] L. Fiorentini, Nonlinear adaptive controller design for air-breathing hypersonic vehicles, Ph.D. Dissertation, Electrical and Computer Engineering Dept., The Ohio State Univ., Columbus, Ohio, 2010.

[16] Z. Pu, R. Yuan, X. Tan, and J. Yi, An integrated approach to hypersonic entry attitude control, *International Journal of Automation and Computing*, 11(1): 39-50, 2014.